

# Liquid–Liquid Equilibria in Binary Solutions Formed by [Pyridinium-Derived][F<sub>4</sub>B] Ionic Liquids and Alkanols: New Experimental Data and Validation of a Multiparametric Model for Correlating LLE Data

Fernando Espiau,<sup>†</sup> Juan Ortega,<sup>\*,†</sup> Lu s Fern andez,<sup>†</sup> and Jaime Wisniak<sup>‡</sup>

<sup>†</sup>Laboratorio de Termodin mica y F sicoqu mica de Fluidos, Parque Cient fico-Tecnol gico, Universidad de Las Palmas de Gran Canaria, Canary Islands, Spain

<sup>‡</sup>Department of Chemical Engineering, Ben-Gurion University of the Negev, Beer-Sheva 84105, Israel

**S** Supporting Information

**ABSTRACT:** Experimental solubility data are presented for a set of binary systems composed of ionic liquids (IL) derived from pyridium, with the tetrafluoroborate anion, and normal alcohols ranging from ethanol to decanol, in the temperature interval of 275–420 K, at atmospheric pressure. For each case, the miscibility curve and the upper critical solubility temperature (UCST) values are presented. The effects of the ILs on the behavior of solutions with alkanols are analyzed, paying special attention to the pyridine derivatives, and considering a series of structural characteristics of the compounds involved. Miscibility curves are modeled using, for the first time in a LLE study, an adimensional form of a semiempirical model proposed for the Gibbs excess function,  $G^E = G^E(p, T, x)$  [*Ind. Eng. Chem. Res.* **2010**, *49*, 406], whose particular form in this work is

$$g^E(T, x) = z(x)[1 - z(x)] \sum_{i=0}^r g_i(T)z^i(x)$$

The results are compared with those of an extended form of the Non-Random Two-Liquids (NRTL) equation, using temperature-dependent parameters. In both cases, a rigorous procedure is carried out to calculate the LLE data, considering the isoactivity criteria, and a global test to check the phase stability for the solutions studied. The final evaluation of the application with the new equation gave satisfactory results.

## 1. INTRODUCTION

Because of the interest in the use of ionic liquids (ILs) as solvents in applications in the chemical industry, it is important to know their solubilities with other conventional solvents. More specifically, some pyridine derivatives (such as those used in this work) have produced good results in certain applications, such as sulfur extracting agents,<sup>1</sup> lubricants,<sup>2</sup> and chemical reactions.<sup>3</sup>

Our research group has worked with three isomeric substances having a common nucleus of a pyridine derivative, [butyl-X-methylpyridinium] (X = 2, 3, 4) [tetrafluoroborate],<sup>4–6</sup> and other nonisomeric [butylpyridinium][tetrafluoroborate],<sup>7</sup> using water and several alkanols (methanol to pentanol) as solvents. For some of these mixtures, the miscibility capacities are known; however, these studies are incomplete, because the initial working project included a greater number of alkanols, from methanol to decanol, with the limitations imposed by the variable temperature in experiments carried out at atmospheric pressure. Here, the previous studies are complemented by providing data, and their analysis, for new systems. The main objectives of this work are to provide experimental data for liquid–liquid equilibria (LLE), and their interpretation and modeling. The latter is a fundamental step in the field of dissolutions, where the model is used in specific applications in chemical engineering and that have not yet produced satisfactory results. In case of LLE, and

from previous experience, it is sometimes difficult to apply the mathematical model correctly, because of the presence of broad plateaus on the miscibility curves, making it difficult to estimate these curves accurately in solutions with ILs.

The first stage in this work consisted in constructing a database ( $x_{IL}, T$ ) formed by a set of 14 previously studied systems, with [butyl-X-methylpyridinium] (X = 2, 3, 4) [tetrafluoroborate], or [butylpyridinium][tetrafluoroborate] + alkanol,<sup>4–7</sup> and by a set of twenty-five new binary systems determined experimentally for this work. The literature shows that the data correlation has been mainly performed using the Non-Random Two-Liquids (NRTL) model.<sup>8</sup> However, because of the irregular distribution of the LLE data, there is some difficulty fitting the systems studied, and extended versions of the original model must be used to obtain acceptable correlations. Previous works<sup>9,10</sup> have presented the development and application of a polynomial model for Gibbs excess function  $G^E = \psi\{p, T, z(x)\}$ , which gave good results for the correlation of vapor–liquid equilibrium (VLE) data and other properties of solutions. This model will be

**Received:** July 17, 2011

**Accepted:** September 22, 2011

**Revised:** September 11, 2011

**Published:** October 10, 2011

Table 1. Physical Properties of Pure Compounds<sup>a</sup>

compound	$\rho$ (kg m <sup>-3</sup> )		$n_D$		$\rho = A \exp(-\alpha T)$			$n_D = a + bT$	
	exp.	lit.	exp.	lit.	A	10 <sup>3</sup> ( $\alpha$ ) exp.	10 <sup>3</sup> ( $\alpha$ ) lit.	a	10 <sup>4</sup> (-b)
[bpy][BF <sub>4</sub> ]	1214.04		1.4455		1434.4	0.56	0.56 <sup>d</sup>	1.4748	1
[b2mpy][BF <sub>4</sub> ]	1202.20	1202.17 <sup>s</sup>	1.4540	1.4545 <sup>g</sup>	1417.4	0.55	0.57 <sup>c</sup>	1.5198	2
[b3mpy][BF <sub>4</sub> ]	1182.58	1182.19 <sup>e</sup>	1.4474	1.4473 <sup>e</sup>	1406.4	0.58	0.59 <sup>h</sup>	1.5151	2
[b4mpy][BF <sub>4</sub> ]	1182.84	1183.49 <sup>f</sup>	1.4526	1.4517 <sup>f</sup>	1402.2	0.57	0.58 <sup>h</sup>	1.4952	1
[hpy][BF <sub>4</sub> ]	1155.06		1.4474		1365.3	0.56		1.4818	1
ethanol	785.05	784.93 <sup>b</sup>	1.3595	1.3594 <sup>b</sup>	1109.1	1.16	1.15 <sup>c</sup>	1.4850	4
propan-1-ol	799.70	799.96 <sup>b</sup>	1.3834	1.3837 <sup>b</sup>	1097.0	1.06	1.05 <sup>c</sup>	1.5070	4
butan-1-ol	805.95	805.85 <sup>b</sup>	1.3974	1.3974 <sup>b</sup>	1087.7	1.00	1.00 <sup>c</sup>	1.5205	4
pentan-1-ol	810.97	811.50 <sup>b</sup>	1.4078	1.4080 <sup>b</sup>	1074.6	0.94	0.95 <sup>c</sup>	1.5275	4
hexan-1-ol	815.19	815.34 <sup>b</sup>	1.4160	1.4157 <sup>b</sup>	1071.5	0.92	0.91 <sup>c</sup>	1.5359	4
heptan-1-ol	818.70	818.70 <sup>c</sup>	1.4224	1.4223 <sup>c</sup>	1067.0	0.89	0.89 <sup>c</sup>	1.5409	4
octan-1-ol	821.81	821.57 <sup>b</sup>	1.4272	1.4276 <sup>b</sup>	1065.3	0.87	0.87 <sup>c</sup>	1.5420	4
nonan-1-ol	824.76	824.70 <sup>c</sup>	1.4317	1.4319 <sup>c</sup>	1068.4	0.87	0.86 <sup>c</sup>	1.5466	4
decan-1-ol	826.54	826.30 <sup>c</sup>	1.4347	1.4353 <sup>c</sup>	1068.0	0.86	0.85 <sup>c</sup>	1.5490	4

<sup>a</sup> Comparison with literature values. Density  $\rho$  and refractive index  $n_D$  values were reported at 298.15 K, and thermal coefficients for  $\rho = \rho(T)$  and for  $n_D = n_D(T)$ . <sup>b</sup> Taken taken from ref 12. <sup>c</sup> Taken taken from ref 13. <sup>d</sup> Taken taken from ref 14. <sup>e</sup> Taken taken from ref 4. <sup>f</sup> Taken taken from ref 5. <sup>g</sup> Taken taken from ref 6. <sup>h</sup> Taken taken from ref 15.

used in this work for the first time to study its efficacy in the treatment of liquid–liquid equilibrium (LLE) data, comparing the goodness of fit of the correlation obtained with that obtained via the NRTL model. For a rigorous treatment of LLE data using the two models mentioned, a potent genetic algorithm (GA) is used, which was specially developed for this study, which takes into account the global stability tests as a criterion of solution stability, verified by Marcilla et al.<sup>11</sup>

## 2. EXPERIMENTAL SECTION

**2.1. Materials.** Ionic liquids used in this work contain the common anion tetrafluoroborate [BF<sub>4</sub>]<sup>-</sup> and the following pyridinium-derived cations: [butyl-X-methylpyridinium]<sup>+</sup> (X = 2, 3, 4), [butylpyridinium]<sup>+</sup>, and [hexylpyridinium]<sup>+</sup>. All the ILs were provided by IOLITEC, GmbH & Co. KG, and had a commercial purity of 99+ % w/w. Before use, they were degasified with ultrasound and slow distillation in a rotavapor. The water content was determined with a Model C-20 Karl Fischer coulometric analyzer from Mettler, showing values of <350 ppm in all cases. The ILs were stored and handled, and the mixtures were prepared in a drybox, with a moisture content of <5%. Alkanols of the highest commercial purity were supplied by Aldrich, and before use were degasified for several hours and stored over a 0.3-nm Fluka molecular sieve. The water content of the alkanols was measured using the apparatus described above and gave acceptable values. Nonetheless, the purity of the alkanols was verified by GC, giving values close to those indicated by the manufacturer. The quality of all the products was verified by measuring their densities  $\rho$ , and refractive indices  $n_D$ , at 298.15 K and atmospheric pressure. The values obtained for the ILs and the alkanols were similar to those reported in previous works,<sup>4–7,12–15</sup> (see Table 1). Measurements of  $\rho$  and  $n_D$  were recorded for all products in the interval of 288–328 K, estimating the correlations of these properties in Table 1 as a function of temperature. The comparison of the thermal expansion coefficients was acceptable.

**2.2. Apparatus and Procedures.** Experimental determination of the solubility points of mixtures of ILs + alkanols was carried out in a LLE cell,<sup>4–6</sup> using a procedure of continuous dilution with visual detection of turbidity changes. Measurements were made in the temperature interval of 275–420 K and at atmospheric pressure, while the cell was thermostatted at all times using a Polyscience external circulation thermostat bath with a liquid coolant, with temperature control of  $\pm 0.01$  K, reflected by oscillations in the cell of  $\pm 0.02$  K. The transition temperature was measured with an ASL-F25 thermometer that showed  $\pm 1$  mK. A Model PT100 probe submerged in the liquid showed a reading error of  $\pm 0.03$  K in the measurement of the cell internal temperature. Solubility measurements ( $x_{IL}, T$ ) were initially made putting a known quantity of IL in the cell, adding accurately determined quantities of the corresponding alkanol, using Hamilton Model TLL 100- $\mu$ L precision syringes. These quantities were also estimated from weight differences. A magnetic stirrer facilitated dissolution, with heating and/or cooling, until the phases had been transformed to a single completely homogeneous phase. The temperature at the time of transition was recorded. The operation was repeated several times with known quantities of alkanol. Pairs of values ( $x_{IL}, T$ ) were determined until values close to  $x_{IL} = 0.5$  were obtained. The IL compositions calculated for each point presented an uncertainty of  $\pm 0.001$ . The process was repeated in the opposite direction, introducing a known quantity of alkanol in the cell, to which small quantities of ionic liquid were repeatedly added, and calculating the compositions in the interval  $0.5 > x_{IL} > 0$ . By plotting the new pairs of values ( $x_{IL}, T$ ), the graph started in the previous stage can be completed. All the reagents were handled using the appropriate safety precautions.

## 3. RESULTS

**3.1. Experimental LLE Data.** Table S1 in the Supporting Information shows the experimental  $x_{IL}-T$  data obtained for the following binary systems not studied previously: [butylpyridinium][tetrafluoroborate] + alkan-1-ol (C<sub>5</sub>–C<sub>7</sub>),

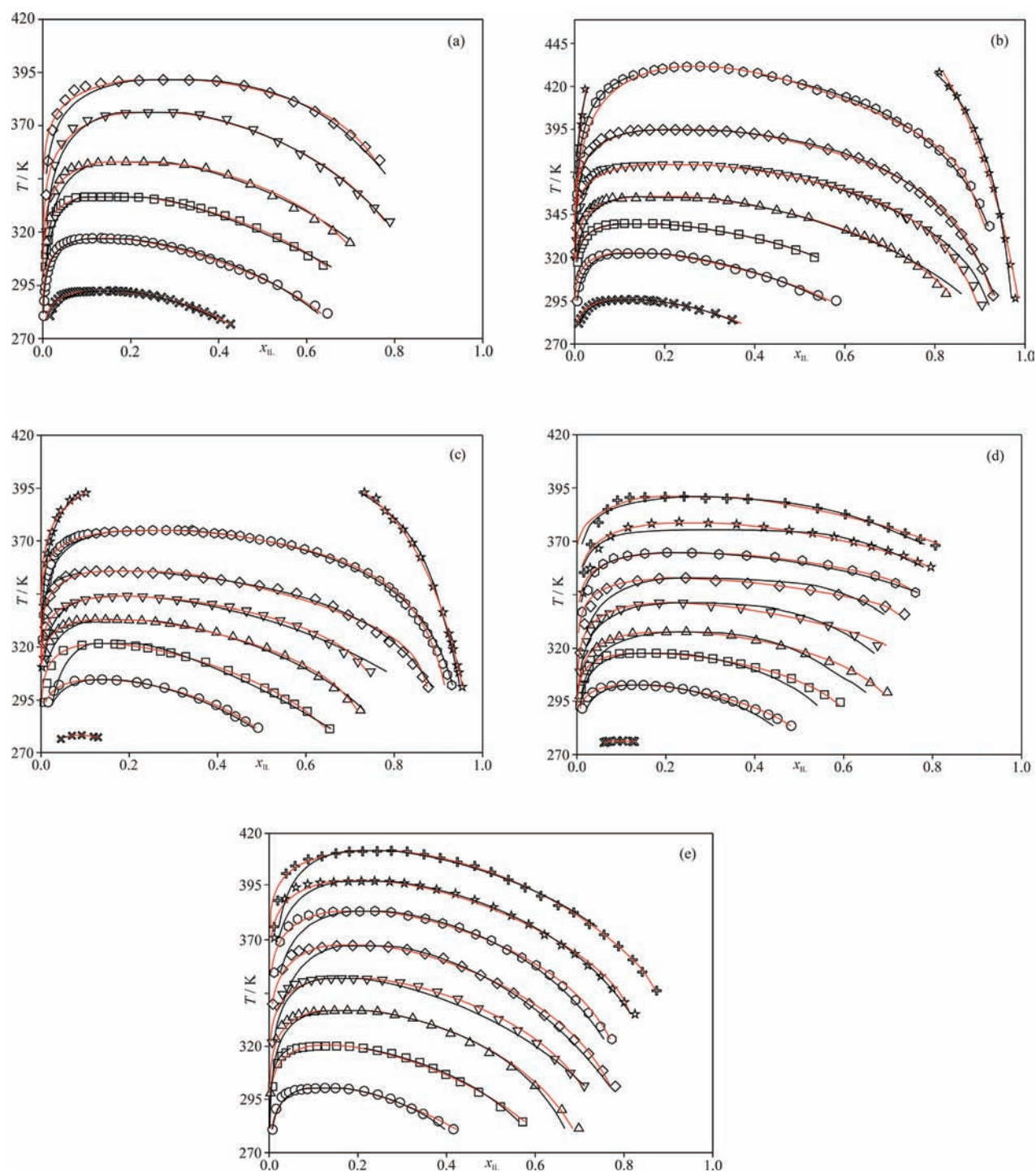


**Figure 1.** Liquid–liquid equilibria (LLE) experimental data ( $x_{IL}, T$ ) for binaries: (a) R = butyl; (b) R = butyl-2-methyl; (c) R = butyl-3-methyl; (d) R = butyl-4-methyl, and (e) R = hexyl.  $x_{IL}[\text{R-py}][\text{BF}_4] + (1 - x_{IL})$  alkanol and miscibility curves determined by eq 10 (red line) and eq 16 (black line). Legend: (hollow X) ethanol; (O) propan-1-ol; (□) butan-1-ol; (Δ) pentan-1-ol; (▽) hexan-1-ol; (◇) heptan-1-ol; (○) octan-1-ol; (☆) nonan-1-ol; and (hollow cross) decan-1-ol.

[butyl-2-methyl-pyridinium][tetrafluoroborate] + alkan-1-ol ( $C_6$ – $C_9$ ), [butyl-3-methyl-pyridinium][tetrafluoroborate] + alkan-1-ol ( $C_5$ – $C_9$ ), [butyl-4-methyl-pyridinium][tetrafluoroborate] + alkan-1-ol ( $C_6$ – $C_{10}$ ), [hexylpyridinium][tetrafluoroborate] + alkan-1-ol ( $C_3$ – $C_{10}$ ). The database generated was used together with data published previously<sup>4–7</sup> to achieve one of the objectives of this work, to treat and correlate them using two models:

the NRTL model<sup>8</sup> and a parametric model proposed by the authors in previous works<sup>9,10</sup> (detailed in the following section). The graphs in Figures 1a–e show the results for the set of compounds studied, with the distribution of experimental points obtained for each of the ILs. It can be seen that all the systems have the same binodal curve typology, with an Upper Critical Solubility Temperature (UCST) presenting a quasi-regular

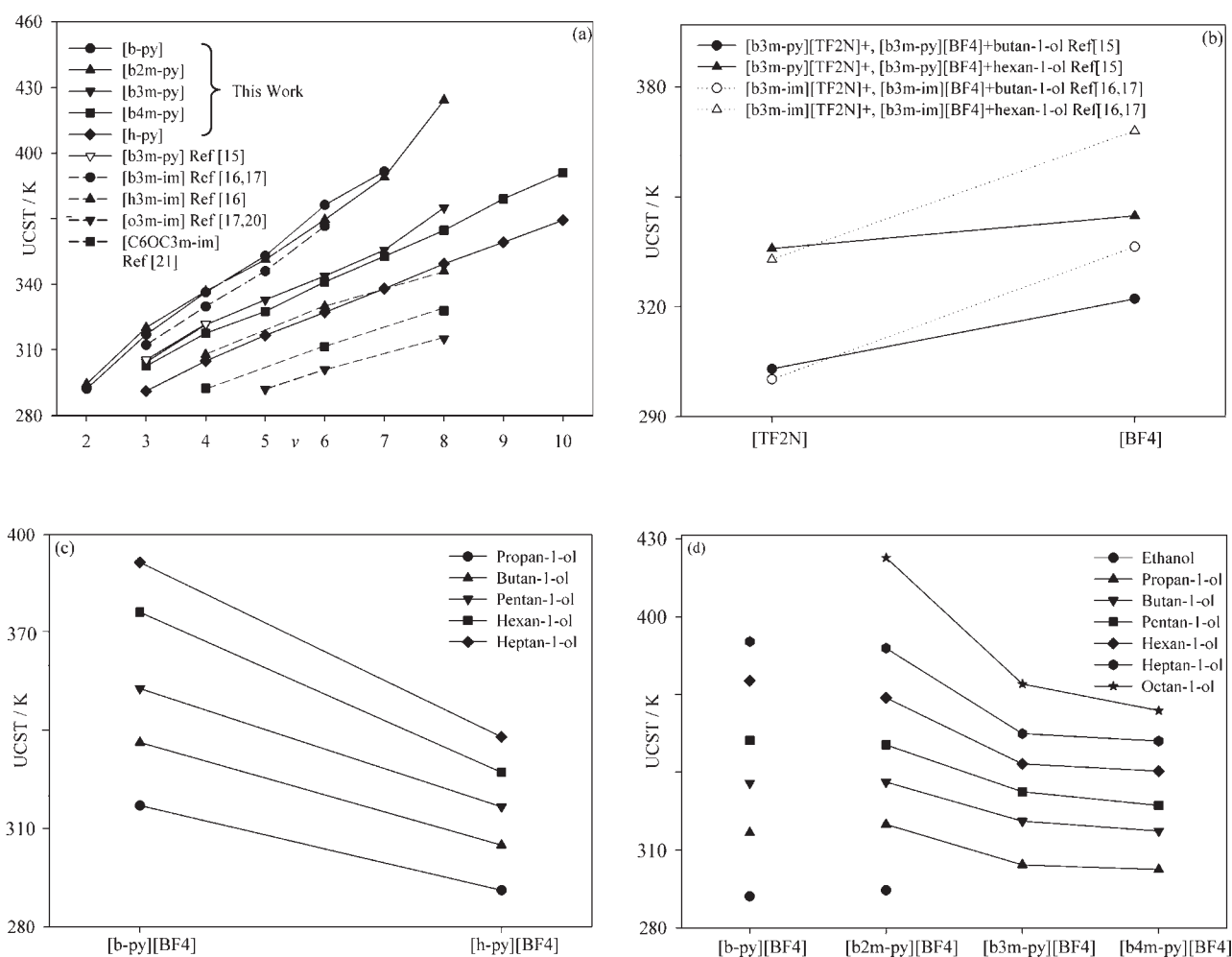


**Figure 2.** (a) Plots indicating the variation of the UCST as a function of the number of carbons ( $\nu$ ) in the binaries IL +  $C_nH_{2n+1}(OH)$  (for pyridinium-derived ILs (solid black line) and for imidazolium-derived ILs (dashed black line)). (b) Plots indicating the variation of the UCST as a function of the nature of the anion in the binaries ([b3m-py][BF<sub>4</sub>], or [b3m-py][TF<sub>2</sub>N] + alkan-1-ol ( $\nu = 4, \nu = 6$ ) (solid black line) and [b3m-im][BF<sub>4</sub>], or [b3m-im][TF<sub>2</sub>N] + alkan-1-ol ( $\nu = 4, \nu = 6$ ) (dashed black line)). (c) Plots indicating the variation of the UCST as a function of the alkyl chain length of [R-py][BF<sub>4</sub>]. (d) Plots indicating the variation of the UCST as a function of the the position of methyl group X in the IL, in the binaries [bXmpy][BF<sub>4</sub>] + alkan-1-ols.

variation with the alkanol chain (Figure 2a). Another qualitative feature is evident in Figures 1a–e: over a short interval of compositions lower than the UCST,  $[0 < x_{IL} < x_{IL,UCST}]$ , very low compositions of IL are recorded with  $x_{IL}$  values higher than the uncertainty assigned previously for the  $x_{IL}$  and the opposite occurs in the interval  $[x_{IL,UCST} < x_{IL} < 1]$ . The behavior for all the curves shown in Figures 1a–e coincides with that of other IL–alkanol systems and permits a brief analysis of the regular behavior of the UCST with the different nature of the compounds involved in the different LLE (see discussion below).

**3.2. Interpretation of Experimental Results.** The experimental data obtained can help to make a brief analysis of the behavior of binary systems, based on different aspects that characterize the nature of the ILs used, and the factors affecting the solutions chosen. The most important aspects to be taken into account are:

- the nature of the ionic cation/anion groups,
- the functional groups that are added to each of these, and
- the chain lengths and the position of the groups in the organic part of the IL.

The experimental work has been carried out with several ILs with a common cation, and a central core derived from pyridium. Hence, the analysis must especially focus on the aspects mentioned in aspect (c), which is shown later. Nonetheless, from the aspects mentioned in (a) and (b), comparative observations can be made that can help to interpret the systems' behavior.

Regarding the anion, in relation to the same pyridium-derived ILs studied here, the literature<sup>16</sup> reports data for [butyl-3-methylpyridinium] [bis(trifluoromethylsulfonyl)imide] + alkanol ( $C_4, C_6$ ), and the following order can be observed, for the same alkanols, for the miscibility curves as a function of the anion of the IL: [bis(trifluoromethylsulfonyl)imide] < [tetrafluoroborate] see Figure 2b, which shows that the anion/cation interaction of the former are weaker and are able to easily form hydrogen bonds with the alkanols, giving rise to greater mutual solubilities, with miscibility curves and UCST values lower than those recorded for the [cation]<sup>+</sup>[tetrafluoroborate]<sup>−</sup>. The same applies to analogous mixtures but with imidazolium derivatives.<sup>17,18</sup>

In a brief comparison of the cation in relation to its chemical nature, leaving the influence of the alkyl chain bonded with the

pyridine ring [R–py], and their position, to be analyzed in a separate section, it can be said that experimental studies mainly based on compounds with cations derived from imidazolium and pyridium do not present any clear tendency, since this factor depends on the type of anion concerned. Hence, the mutual solubilities of the alkanols in [butyl-methylpyridinium][bis(trifluoromethylsulfonyl)imide] are greater than in [butyl-methylimidazolium][bis(trifluoromethylsulfonyl)imide], showing a clear influence of the larger size of the pyridium-derived cation versus the imidazolium-derived one, the former improving the miscibility of the solution. However, this does not occur with the [tetrafluoroborate] anion, for which there is a reduction in the biphasic composition regions in the order of [butyl-3-methylimidazolium] < [butyl-3-methylpyridinium], as shown in Figure 2b.

**3.2.1. Influence of the Alkanol Chain on Miscibility Curves.** Figures 1a–e shows that, at the same temperature, the composition corresponding to mutual solubility in the interval  $[0 < x_{IL} < x_{IL,UCST}]$  decreases with increasing alkanol chain length, because of a decrease in its polar character. The latter factor increases the tendency to immiscibility. This is shown in Figure 2a, which reports the changes in UCST of each binary mixture of IL + alkanol, for a same alkanol, versus the number of carbons in the linear alkanol. This result can also be observed in mixtures of a similar nature in which the IL contains the [tetrafluoroborate]<sup>−</sup> anion, as reported by others. This observation can be applied to the systems: [butyl-3-methyl-imidazolium][tetrafluoroborate] + alkanol,<sup>17,19</sup> [butyl-3-methyl-pyridinium][tetrafluoroborate] + alkanol,<sup>16</sup> [hexyl-3-methylimidazolium][tetrafluoroborate] + alkanol,<sup>17,20</sup> [octyl-3-methylimidazolium][tetrafluoroborate] + alkanol,<sup>18,21</sup> and [hexyloxymethyl-3-methylimidazolium][tetrafluoroborate] + alkanol.<sup>22</sup> Moreover, a similar behavior is observed in mixtures in which the IL presents a different anion than the [tetrafluoroborate]<sup>−</sup>, for example, [butyl-3-methylpyridinium]-[bis(trifluoromethylsulfonyl)imide] + alkanol,<sup>16</sup> [ethyl-3-methylimidazolium][bis(trifluoromethylsulfonyl)imide] + alkanol,<sup>23,24</sup> [ethyl-3-methylimidazolium][hexafluorophosphate] + alkanol,<sup>25</sup> [butyl-3-methylimidazolium][hexafluorophosphate] + alkanol,<sup>19,26–29</sup> [hexyl-3-methylimidazolium][hexafluorophosphate] + alkanol,<sup>26,29</sup> [hexyl-3-methylimidazolium][bis(trifluoromethylsulfonyl)imide] + alkanol,<sup>18,30</sup> [octyl-3-methylimidazolium][hexafluorophosphate] + alkanol,<sup>29</sup> [ethyl(2-hydroxyethyl)dimethylammonium][bis(trifluoromethylsulfonyl)imide] + alkanol,<sup>31</sup> [tetrabutylphosphonium]-[methanesulfonate] + alkanol,<sup>32</sup> and [hexyloxymethyl-3-methylimidazolium][bis(trifluoromethylsulfonyl)imide] + alkanol.<sup>22</sup> In summary, the mutual solubility of the IL–alkanol system decreases as  $\nu$  increases in  $C_{\nu}H_{2\nu+1}(OH)$ , accompanied by a rise in the UCST value.

**3.2.2. Variation of the UCST with the Alkyl Chain of the IL Cation.** Special attention should be paid to the length of the R chain in [tetrafluoroborate][R–py] and/or its possible branches. The following observations can be made about the influence of the variation in cation chain and the different position of the alkyl group in the pyridine ring. There are a few studies in the literature on miscibility in binary mixtures of IL + alkanol, where the IL is formed by cation = [pyridine derivatives]<sup>+</sup> and anion = [tetrafluoroborate]<sup>−</sup>, which could be used to carry out an exhaustive analysis on the evolution of binodal curves as a function of alkyl chain length of cation. The information presented in this work permits one to declare that an increase in alkyl chain length of the cation leads to a decrease of the UCST,<sup>17,18,33</sup> for the same alkanols, as shown in Figure 2c, for

mixtures of [butylpyridinium][tetrafluoroborate] and [hexylpyridinium][tetrafluoroborate]. In other words, the mutual solubility between IL–alkanol at a given temperature increases with the cation chain length, probably due to an increase in the IL/alkanol contact surfaces and van der Waals interactions. This results in an increased mutual solubility of these solutions, and the corresponding decrease in the UCST. This result has been shown by other authors<sup>17,18</sup> in studies on the binary mixtures alkanol + [butyl-3-methylimidazolium][tetrafluoroborate], or + [hexyl-3-methylimidazolium][tetrafluoroborate], or + [octyl-3-methylimidazolium][tetrafluoroborate], and for mixtures of [butyl-3-methylpyridinium][bis(trifluoromethylsulfonyl)imide] and [hexyl-3-methylpyridinium][bis(trifluoromethylsulfonyl)imide] + alkanol.<sup>16</sup>

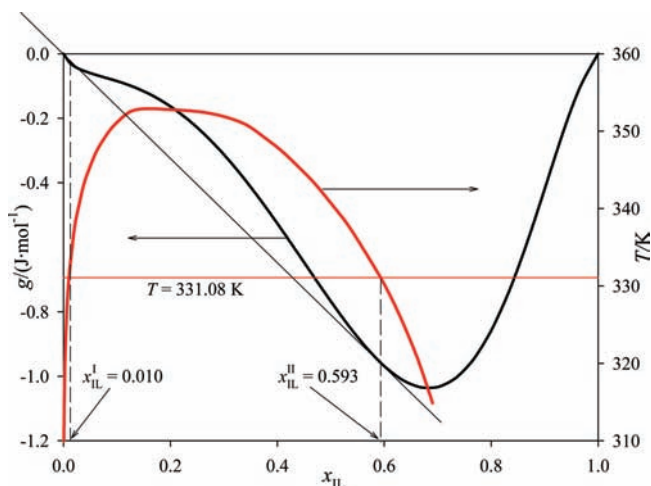
**3.2.3. Variation in the Position of the Methyl Group in the Pyridine Ring.** The set of binary mixtures considered here for IL + alkanol, for which data have already been published,<sup>4–7</sup> can be used to study the evolution of the miscibility zones and the tendencies presented by their maxima, UCST, and biphasic regions, in relation to the position occupied by the methyl group in the pyridine ring.

Figure 2d shows the variation in UCST for mixtures of alkanol + [butylpyridinium][tetrafluoroborate], alkanol + [butyl-2-methylpyridinium][tetrafluoroborate], alkanol + [butyl-3-methylpyridinium][tetrafluoroborate], and alkanol + [butyl-4-methyl pyridinium][tetrafluoroborate] versus the cation of the IL in the order [butylpyridinium] < [butyl-2-methylpyridinium] < [butyl-3-methylpyridinium] < [butyl-4-methylpyridinium], with values belonging to mixtures of isomeric ILs being joined by a continuous line to the same alkanol. The results show that, for a given alkanol, the UCST of the solution decreases with the position of the CH<sub>3</sub>– group in the pyridine ring. An exception to this rule is for mixtures with [butylpyridinium][tetrafluoroborate], since this is not an isomer of the others; in other words, it has “zero” CH<sub>3</sub>– groups bound to the central nucleus.

Hence, Figure 2d clearly shows a regular decrease in the UCST value, which is lower in the IL group with the *para*- position, since the lengthening of the molecule permits a better physical accommodation of the compounds in the final solution. This accommodation becomes more difficult for the *meta*- and *ortho*- positions.

#### 4. THERMODYNAMIC–MATHEMATICAL ANALYSIS: DATA CORRELATION

The distribution of solubility data presented in Table S1 in the Supporting Information and in Figures 1a–e would lead one to expect certain difficulties in obtaining a good correlation. Therefore, the data were adjusted with two models: NRTL,<sup>8</sup> which is one of the models most used in phase equilibrium studies, especially in the study of solutions with ionic liquids, and where the goodness of fit obtained can be used to check the value of another model, which consists in a polynomial expression previously used by the authors of this work to treat vapor–liquid equilibria (VLE) data and other properties, with excellent results.<sup>9,10</sup> The latter is established for Gibbs' excess function, which is related to the active fraction  $z$  and is also a function of composition and temperature since, here, the isobaric behavior is analyzed. The procedure used for both models is designed to strictly comply with the isoactivity criterion and to guarantee the stability of the solution established with conjugate compositions.



**Figure 3.** Representation of the Gibbs function,  $g = g^E + g^{\text{ideal}}$  (solid black line), at  $T = 331.08$  K obtained by eq 10 applied to LLE data for the system [b-py][BF<sub>4</sub>] + pentan-1-ol, and where the tangent line define the conjugate compositions,  $x_{\text{IL}}^{\text{I}}$  and  $x_{\text{IL}}^{\text{II}}$ , for the two phases. The red line represents the LLE fitting curve for the binary described above and using the model proposed.

In binary solutions, the curve that describes Gibbs' energy function, or that corresponding to the adimensional function versus the composition,

$$g = \frac{G}{RT} = \varphi(x_i)$$

plays an important role in establishing the necessary condition to ensure the stability of phases. Hence, at different fixed values of pressure, temperature, and composition for the binary mixture  $x_1$ , the solution is absolutely stable if, and only if, all the points of  $g$  are above the tangent straight line to this curve at  $x_1$ . By contrast, there will be concentration intervals in which the following is true:

$$\left( \frac{\partial^2 g}{\partial x_1^2} \right)_{p,T} < 0 \quad (1)$$

in which the extreme values coincide with compositions where curve  $g$  reaches points of inflection, and some points on this curve will share the same tangent straight line. For a binary mixture, the Gibbs molar energy can be expressed as

$$g = \frac{G}{RT} = \frac{G^E}{RT} + \frac{G^{\text{ideal}}}{RT} = g^E + (x_1 \ln x_1 + x_2 \ln x_2) \quad (2)$$

These comments are graphically represented in Figure 3 for one of the systems studied, namely, [bpy][BF<sub>4</sub>] + pentan-1-ol. The black line characterizes the  $g$ -function at a temperature of 331.08 K calculated by the proposed model, according to the procedure indicated below; the red line represents the miscibility curve for that binary—and the corresponding isothermal—observing how the points tangent to the  $g$ -curve coincide with the LLE compositions at that temperature. Now, considering the variation of a set of situations shown in Figure 3 with temperature (for different values of  $T$ ), a succession of conjugate compositions is generated, creating a surface in a three-dimensional (3D) diagram (see Figure 4).

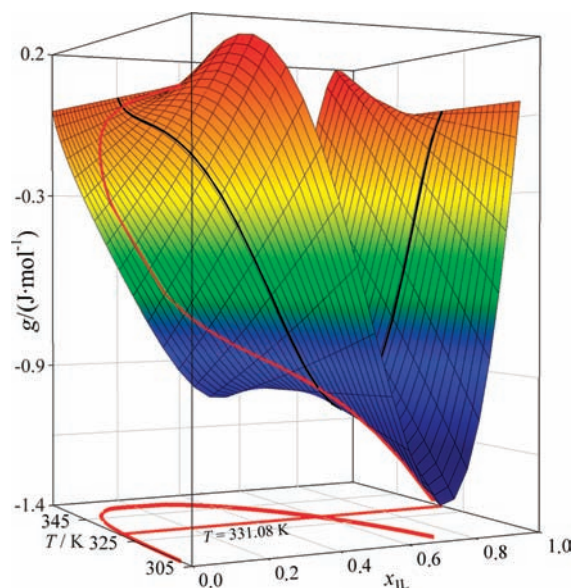


**Figure 4.** Three-dimensional (3D) diagram for the function  $g = g(T, x_{\text{IL}})$  obtained using the model proposed in this work for the mixture [b-py][BF<sub>4</sub>] + pentan-1-ol, indicating the isothermal curve (solid black line) at 331.08 K and the red line on the surface, which is generated by the set of points corresponding to the shaft between that surface and the tangent lines under isothermal conditions. The projection on the  $T$ - $x_{\text{IL}}$  plane of the 3D trajectory creates a curve of the conjugate compositions of LLE for the binary indicated in Figure 3.

The condition expressed by eq 1 can also be expressed as a function of the Gibbs molar excess energy, instead of Gibbs molar energy of the mixture, giving rise to the following condition of instability, with the presence of two phases:

$$\left( \frac{\partial^2 g^E}{\partial x_1^2} \right)_{p,T} + \frac{1}{x_1 x_2} < 0 \quad \text{or} \quad \left( \frac{\partial^2 G^E}{\partial x_1^2} \right)_{p,T} + \frac{RT}{x_1 x_2} < 0 \quad (3)$$

In the analysis of a general situation—e.g., the case of a solution at  $p_j$  and  $T_j$ , which has reached a state of equilibrium  $j$ , and that presents composition values that satisfy the condition expressed by eq 3—will present immiscibility with separation into two liquid phases, I and II, where the conjugate compositions for compound 1,  $x_{1j}^{\text{I}}$  and  $x_{1j}^{\text{II}}$ , will coincide with points on the  $g$ -curve that have the same tangent line. In the case of LLE, the thermodynamic equilibrium condition of equal chemical potentials in the phases where the component is present, can be relaxed to one of equal activity, since both phases are liquid. For a binary mixture, the mathematical model of LLE presents, for each state of equilibrium  $j$ , a system of equations for each pair of conjugate compositions, or tielines, determined experimentally as follows:

$$\left. \begin{aligned} x_{1j}^{\text{I}} \gamma_1^{\text{I}}(x_{1j}^{\text{I}}, p_j, T_j) &= x_{1j}^{\text{II}} \gamma_1^{\text{II}}(x_{1j}^{\text{II}}, p_j, T_j) \\ x_{2j}^{\text{I}} \gamma_2^{\text{I}}(x_{1j}^{\text{I}}, p_j, T_j) &= x_{2j}^{\text{II}} \gamma_2^{\text{II}}(x_{1j}^{\text{II}}, p_j, T_j) \end{aligned} \right\} \quad (4)$$

where  $\gamma_i^\alpha$  represents the activity coefficient of the compound  $i$  in phase  $\alpha = \text{I, II}$ .

To calculate the parameters of the model chosen for the activity coefficients, the criteria described in the literature<sup>11</sup> have

been applied. For this purpose, we have used the two-stage iterative procedure described in the flow diagram given in Figures A1 and A2 in the Appendix. The first stage uses the necessary but insufficient isoactivity condition, and the second one uses minimization of the compositional differences between the experimental and calculated phases. Optimization problems, established in these two stages, were carried out by applying an evolutionary technique based on a genetic algorithm (GA), which guarantees the attainment of global solutions to these problems. The characteristics of these global algorithms are similar to those of others constructed for the joint correlation of different thermodynamic properties, and some of their applications to other cases, which have been presented in previous works.<sup>9,10</sup> The detailed stages of this procedure are as follows:

- (1) Initial values are calculated for the model parameters obtained by optimizing an objective function (OF)<sub>γ</sub>, based on the isoactivity criterion and expressed as

$$(\text{OF})_{\gamma} = \sum_{j=1}^m \sum_{i=1}^2 \left[ x_{ij}^I \gamma_i(x_{ij}^I, p_j, T_j) - x_{ij}^{II} \gamma_i(x_{ij}^{II}, p_j, T_j) \right]^2 \quad (5)$$

and using the experimental molar fractions of each species in both liquid phases.

- (2) The values thus obtained are now used in a second stage in which they are optimized in an iterative manner by minimizing a new objective function based on the differences between the corresponding experimental conjugate compositions,  $x_{ij, \text{exp}}^I$  and  $x_{ij, \text{exp}}^{II}$ , and the calculated values,  $x_{ij, \text{cal}}^I$  and  $x_{ij, \text{cal}}^{II}$ , using the parametric model adapted for activity coefficients:

$$(\text{OF})_x = \sum_{j=1}^m \sum_{i=1}^2 \left[ (x_{ij, \text{exp}}^I - x_{ij, \text{cal}}^I)^2 + (x_{ij, \text{exp}}^{II} - x_{ij, \text{cal}}^{II})^2 \right] \quad (6)$$

This procedure guarantees that the fitting procedure is designed to obtain the set of parameters that determines the real conjugate compositions that are closest, as a set, to the  $m$  experimental values. Since the experimental solubility data presented in Table S1 in the Supporting Information do not include the conjugate compositions for each temperature, which would permit use the above objective functions (OF)<sub>γ</sub> and (OF)<sub>x</sub>, these data must be interpolated to get values for the equilibrium compositions of the first compound in both phases. In this second stage, the algorithm is applied with the mass evaluation of (OF)<sub>x</sub> for each set of parameters, proposed as a partial solution to the minimization problem, and then the  $x_{ij, \text{cal}}^I$  and  $x_{ij, \text{cal}}^{II}$  for each set of parameters, can be calculated. The validity of the procedure presented so far lies in the fact that these calculated molar fractions correspond to *real* equilibrium compositions. One way of guaranteeing this requirement, as applied in this work, consists of determining these molar fractions by resolving the set of equations given as eq 4 with current values of the parameters of the model (for each  $p$  and  $T$  for which experimental data have been determined), to establish the tielines calculated by the model. These  $2 \times 2$  systems of nonlinear equations then are resolved using a conventional Newton–Raphson type iterative procedure. As mentioned previously, this isoactivity criterion is a *necessary but insufficient* condition to ensure the stability of the phases in the compositions calculated. Moreover, there is no guarantee that there is a unique solution to the set of equations described by eq 4, which we have used to determine these

compositions. A more rigorous method entails a partial analysis of the stability of the solutions calculated. This analysis is based on eq 3, or by using the activity coefficients as a condition of stability in each phase of a binary mixture, as shown below.

$$\left( \frac{\partial \ln \gamma_1}{\partial x_1} \right)_{p, T} + \frac{1}{x_1} > 0 \quad \text{or} \quad \left( \frac{\partial \ln \gamma_2}{\partial x_1} \right)_{p, T} + \frac{1}{x_2} > 0 \quad (7)$$

The correlation procedure for the LLE data described will be operative after suitable models have been adopted for the activity coefficients. In recent studies,<sup>9,10</sup> we have discussed the utility of a parametric model, of the type  $G^E = G^E(p, T, x)$ , for the Gibbs excess function in multicomponent systems, of the form

$$G^E(p, T, x) = z_1 z_2 [g_0(p, T) + g_1(p, T) z_1(x) + g_2(p, T) z_1^2(x)] \quad (8)$$

where

$$g_i(p, T) = g_{i1} + g_{i2} p^2 + \frac{g_{i4}}{T} + g_{i3} p T + g_{i5} T^2 \quad \text{and} \quad z_1 = 1 - z_2 \quad (9)$$

In this work, LLE data were determined at constant pressure, so this version of the model can be simplified, by either making  $p = 101.32$  kPa, or by removing the intensive property from eq 9. Selecting the second option leads to the following version of the model, which has been adapted to the isobaric case:

$$\frac{G^E}{RT}(x_1, T) = g^E(x_1, T) = z_1 z_2 \sum_{i=0}^r g_i(T) z_1^i \quad (10)$$

In this work, we have used this dimensional form for the Gibbs function. Therefore, those corresponding to eq 9 will be modulated by the factor  $RT$ . The variation as a function of temperature is generated through the active fractions as follows:

$$z_1 \equiv z_1(x_1, T) = \frac{x_1}{x_1 + k(T)x_2} \quad (11)$$

The corresponding expressions for the activity coefficients are

$$\left. \begin{aligned} \ln \gamma_1(x_1, T) &= z_1 z_2 \sum_{i=0}^r g_i(T) z_1^i + \frac{k(T)x_2}{[x_1 + k(T)x_2]^2} Y(x_1, T) \\ \ln \gamma_2(x_1, T) &= z_1 z_2 \sum_{i=0}^r g_i(T) z_1^i - \frac{k(T)x_1}{[x_1 + k(T)x_2]^2} Y(x_1, T) \end{aligned} \right\} \quad (12)$$

where

$$Y(x_1, T) = (1 - 2z_1) \sum_{i=0}^r A_i(T) z_1^i + z_1 z_2 \sum_{i=1}^r i A_i(T) z_1^{i-1} \quad (13)$$

One of the outstanding characteristics of the polynomial model (eq 8) is its flexibility, which can be understood as the capacity to adapt its formal elements to the experimental data for which a correlation is desired. Inspection of the miscibility curves in Figures 1a–e shows that the experimental data are largely homogeneous, with wide composition intervals, presenting very slight differences between the equilibrium temperatures, even at the critical point UCST. This results in wide plateaus at the top of

the curves, which become even wider with increasing alkanol chain length. This feature makes it difficult to correlate the data, and it shows the need for models with a sufficient capacity for adaptation. Hence, in this work, for modeling by eq 8, we have opted to use a second degree in the active fraction  $z(x)$ , with only the first three terms of eq 9 as temperature-dependent coefficients. Since pressure remains constant, the final form is

$$g_i(T) = \frac{g_{i1}}{T} + g_{i2} \quad (14)$$

Some comments have previously been made in previous studies<sup>9,10</sup> about the parameter  $k(T)$  that appears in expression of eq 11 of the model. It was found that the best results are obtained when this parameter is independent of temperature ( $k(T) \equiv k$ ). The best results were obtained in the global fitting process, together with the other  $g_{ij}$  of the model. The correlation of solubility data for each of the binary mixtures in the study produced optimum values for the model parameters expressed by eq 10, with the standard errors shown in Table S2 in the Supporting Information), and calculated using the following expression:

$$s_x = \sqrt{\frac{\sum_{j=1}^m (x_{1j}^I - \hat{x}_{1j}^I)^2 + (x_{1j}^{II} - \hat{x}_{1j}^{II})^2}{2m}} \quad (15)$$

where  $m$  is the number of experimental points. Figure 5a reports the values of parameter  $k$  for each of the mixtures studied in relation to alkanol chain length. The variation of these parameters presents an increasing tendency when the LLE data are correlated, which is in agreement with its regular variation when determined in relation to certain thermodynamic quantities (see refs 9 and 10). Figures 1a–e illustrates the curves obtained with the model for each of the systems, and they show an acceptable representation of the solubility points. The standard deviations reported in Table S2 in the Supporting Information give a quantitative picture of the excellent behavior of the model (eq 10), despite the apparent initial problems with the distribution of the points. Figure 6 shows a 3D representation of the stability analysis of mixtures [bpy][BF<sub>4</sub>] + alkanol (C<sub>2</sub>–C<sub>7</sub>) with the three quantities  $x_{1L}$ ,  $T$ ,  $E$  (where  $E$  is the condition imposed by eq 3). The values of  $E$  are calculated using eq 8 and

the parameters from Table S2 in the Supporting Information, and compliance of the phase stability condition is verified for the systems indicated. A better observation of stability condition is represented on the  $E$ – $x_{1L}$  plane.

To assess the behavior of the proposed model, the data were also correlated with the NRTL model:<sup>8</sup>

$$\frac{G^E}{RT}(x_1, T) = x_1 x_2 \left( \frac{\tau_{21} G_{21}}{x_1 + G_{21} x_2} + \frac{\tau_{12} G_{12}}{G_{12} x_1 + x_2} \right) \quad (16)$$

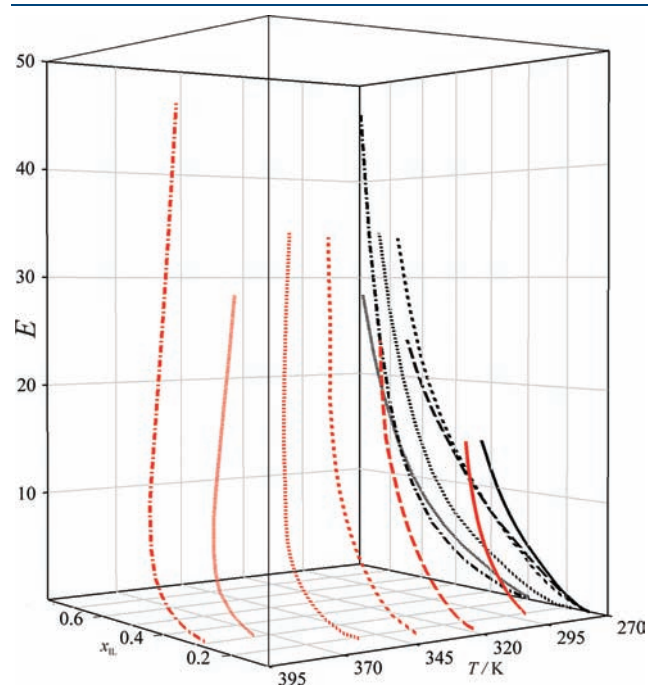


**Figure 6.** Plots of the curves representing the stability analysis of the conjugate compositions calculated by the model proposed in this work (eq 10, represented in red), and the corresponding projections on  $x_{1L}$ – $E$  plane (represented in black) for the binaries: [bpy][BF<sub>4</sub>] + alkanol. (Legend: (solid red line) ethanol, (long dashed red line) propan-1-ol, (hyphenated red line) butan-1-ol, (short dashed line) pentan-1-ol, (dotted red line) hexan-1-ol, and (dash-dotted red line) heptan-1-ol.)  $E = (\partial^2 g^E / \partial x_1^2) + [1/(x_1 x_2)]$ .

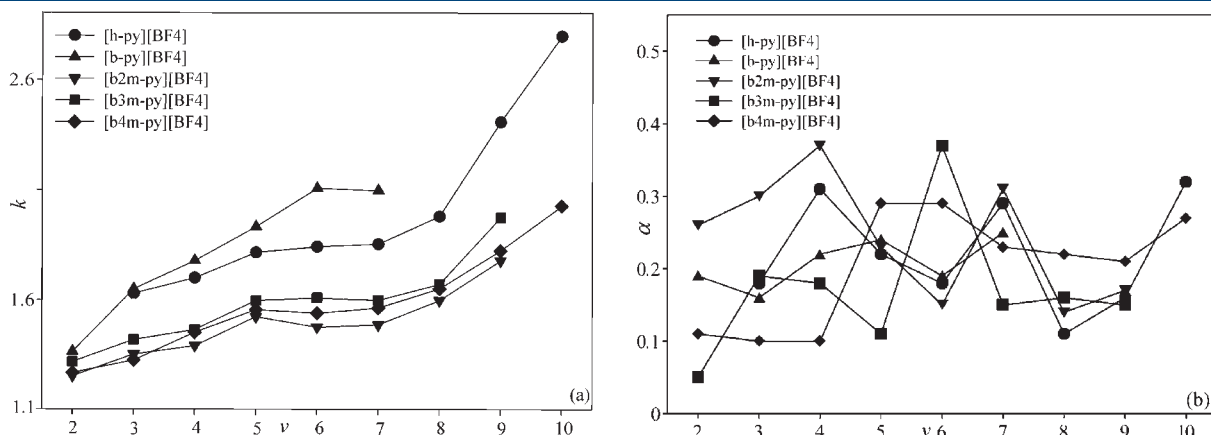


**Figure 5.** Representation of the values for (a) parameter  $k$  and (b) parameter  $\alpha$ , obtained correlating the experimental data ( $x_{1L}, T$ ) of the mixtures studied, according to eqs 10 and 16, respectively, as a function of alkanol chain length,  $\nu$  in C <sub>$\nu$</sub> H<sub>2 $\nu$ +1</sub>(OH).

where

$$\left. \begin{aligned} \tau_{ij} &= \frac{\Delta g_{ij}}{RT} = \Delta g_{ij1} + \frac{\Delta g_{ij2}}{T} + \Delta g_{ij3} \ln T \\ G_{ij} &= \exp(-\alpha \tau_{ij}) \end{aligned} \right\} \quad (17)$$

Because of the special characteristics of the distribution of experimental points, we considered using an extended form for the  $\tau_{ij}$  coefficients, as proposed previously by other authors.<sup>34,35</sup> The set of adjustable model parameters are composed of both the coefficient of nonrandomness  $\alpha$  and the coefficients  $\Delta g_{ij1}$ ,  $\Delta g_{ij2}$ , and  $\Delta g_{ij3}$ , which model the variation in molecular interactions with temperature. The generic expression for activity coefficients obtained from eq 16, which are used directly in each stage of the LLE data correlation procedure followed here, are shown below:

$$\ln \gamma_i(x_i, T) = x_j^2 \left[ \tau_{ji} \left( \frac{G_{ji}}{x_i + G_{ji}x_j} \right)^2 + \frac{\tau_{ij}G_{ij}}{(G_{ij}x_i + x_j)^2} \right] \quad (18)$$

The procedure used to correlate data was identical to that described for the model proposed by eq 8. The same application (described in detail in the Appendix) was used in both cases. Quantitative results of the fits carried out with this model, the values of the parameters and the standard errors associated with the compositions (eq 15) are reported for each binary mixture in Table S2 in the Supporting Information. The parameter  $\alpha$  was considered as an additional parameter estimated in the same correlation procedure. For all the systems, the values of  $\alpha$  oscillate nonregularly from 0.1 to 0.39 (see Figure 5b), except for the system [butyl-3-methylpyridinium][tetrafluoroborate] + ethanol, which presents a value of 0.05. In other words, the systems present values within the interval recommended in the literature (all the data from the DECHEMA LLE collection have been correlated with  $\alpha = 0.2$ ).

Representations of the curves obtained in the fits of solubility data from the two models are presented together with the experimental data in Figures 1a–e. Qualitatively, important differences are observed, especially at the extreme region, where the NRTL model presents curves that do not exist in the real situation, which are also quantitatively shown in the standard deviations  $s_x$  of the correlations. This analysis is based on trends observed in the experimental data and was the reason behind our decision to use the extended version of the NRTL model. This fact justifies our choice of eq 17, which includes six parameters, as a suitable way of making its interaction coefficients  $\tau_{ij}$  dependent on temperature, and also our decision to make parameter  $\alpha$  an additional adjustable parameter. For the NRTL model, we verified that the use of alternative expressions, with fewer parameters, do not produce acceptable correlations in most of the systems studied here. This is also shown in the literature<sup>16</sup> in binary mixtures of ILs, based on pyridine derivatives and imidazolium with alkanols.

## 5. CONCLUSIONS

This work presents a correlation procedure of composition–temperature solubility data for a set of 38 binary mixtures comprised of five ionic liquid (IL) pyridine derivatives having the common anion [tetrafluoroborate]<sup>−</sup>, and a series of linear chained alkanols (from ethanol to decanol). The  $(x_{IL}, T)$  paired values were

determined with the “cloud point” method to obtain points on the binodal curve in the critical regions that define the miscibility zones. The UCST points determined for each mixture presented a regular increasing tendency with increasing alcohol chain length.

Two correlation models were used for the Gibbs function: one previously employed by the authors to correlate vapor–liquid equilibrium (VLE) data<sup>9,10</sup> and derived thermodynamic quantities, and an extended version of the local composition model (Non-Random Two Liquids, NRTL), for comparative purposes. A correlation method was applied (the same for both models) using a genetic algorithm (GA)<sup>36</sup> as a correlation tool and the appropriate objective functions for this procedure. The rigorous method of fit included two stages: one based on isoactivity criteria and the other guaranteeing solution stability established by the conjugate compositions. In general, the equation proposed here yielded acceptable results slightly better than those obtained with the NRTL model.

## APPENDIX

A genetic algorithm (GA)<sup>36</sup> was used to solve the problem of optimizing the objective functions, (OF) <sub>$\gamma$</sub>  (eq 5) and (OF) <sub>$x$</sub>  (eq 6), proposed in the two stages, which guarantees global solutions.<sup>35</sup> The flowcharts in Figures A1 and A2 reflect the implementation of a GA to solve each of those stages. The GA starts from a set of possible random solutions, “populations”, the size of which (or pop\_size) is fixed by the researcher. Each individual in these populations is a chromosome and represents a solution  $\theta$ , of the optimization problem to be solved, which, in our case, coincides with the specific collection of model parameters adopted, NRTL<sup>16–18</sup> or the model proposed for the activity coefficients,  $\gamma_i(x_i, p, T; \theta)$  (eqs 10 and 14). In the GA, these chromosomes (solutions) are subjected to the genetic operations of crossover and mutation, giving rise to offspring chromosomes (other solutions). On one hand, two progenitor chromosomes combine to produce an offspring; on the other hand, the chromosome code is altered to produce a different one by mutation. In each generation, both the progenitor chromosomes and the offspring are assessed to be used using the objective functions of that chromosome (OF) <sub>$\gamma$</sub> ( $\theta$ ) and (OF) <sub>$x$</sub> ( $\theta$ ). The best chromosomes are selected to produce the following generation, and the others are discarded: after several generations, the GA converges in the best chromosome and, therefore, to the global solution of the problem. Considering the variables (OF) <sub>$\gamma$</sub> ( $\theta$ ) and (OF) <sub>$x$</sub> ( $\theta$ ) as the model parameters chosen to correlate the  $\gamma_i(x_i, p, T; \theta)$ , a limitation is imposed by introducing search intervals. Although, for stage 1, there is no previous information to that included within these intervals, the ones in stage 2 are based on those calculated as a solution (initial seed) from stage 1. After setting these search intervals, taking the set of experimental LLE data as a starting point:  $X = \{(x_{ij}^I, x_{ij}^{II}, p_j, T_j) \mid i = 1, 2; j = 1, \dots, m\}$ , GA operates in a similar way for both stages, and can be followed in Figures A1 and A2:

Step 0: Introduction of data  $X = \{(x_{ij}^I, x_{ij}^{II}, p_j, T_j) \mid i = 1, 2; j = 1, \dots, m\}$

Step 1: A first generation is developed,  $t = 1$ , selecting the pop\_size chromosomes ( $\theta_1^t, \dots, \theta_{\text{pop\_size}}^t$ ) randomly in the established search intervals.

Step 2: The objective ofunction (OF) is assessed for each of these chromosomes.

Step 3: Two progenitor chromosomes are selected ( $\theta_a^t, \theta_b^t$ ), by means of a size 2 tournament, which consists of selecting the best chromosome, minimizing the OF to which it is paired, from two taken randomly from the current population  $t$ .

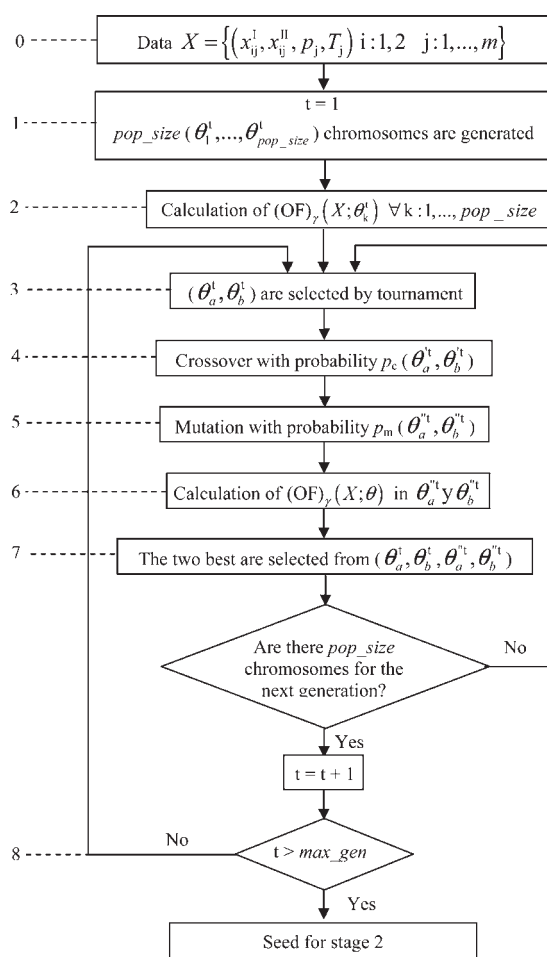


Figure A1. Flow diagram of stage 1.

Step 4: These chromosomes will crossover with probability  $p_{\text{crossover}}$  for which they will take values between 0.6 and 0.8, producing two offspring chromosomes  $(\theta_a^t, \theta_b^t)$ , generated by the convex linear combination of the progenitors.

Step 5: The previous chromosomes will mutate with probability  $p_m$ , with values between 0.1 and 0.2, by arithmetic mutation, producing offspring  $(\theta_a^t, \theta_b^t)$ .

Step 6: The objective function is assessed for each of the chromosomes  $\theta_a^t$  and  $\theta_b^t$ :  $(\text{OF})_\gamma(X; \theta)$  for stage 1 and  $(\text{OF})_x(X; \theta)$  for stage 2.

Step 7: The two best parameters of the set  $(\theta_a^t, \theta_b^t, \theta_a^t, \theta_b^t)$ , considering that their respective associated (OF) values will become the next generation,  $t = t + 1$ .

Step 8: A stopping condition is imposed for the GA corresponding to a given number of generations  $\text{max\_gen}$ .

The steps described present the shared features of both stages, although it is appropriate to describe the main differences between them. The application of the GA in stage 2, steps 2–6, includes the mass evaluation of the function  $(\text{OF})_x$  (eq 6). This entails the calculation of the conjugate compositions,  $x_{ij,\text{cal}}^I$  and  $x_{ij,\text{cal}}^{II}$  for each of these chromosomes solving the system of equations presented as eq 4. Finally, the greater rigor of this method is guaranteed with the stability analysis of the solutions calculated as described here. Figure A2, between steps 5 and 6, shows how the analysis is carried out with stage 2 of the fitting procedure, which is based on the stability condition of eq 7.

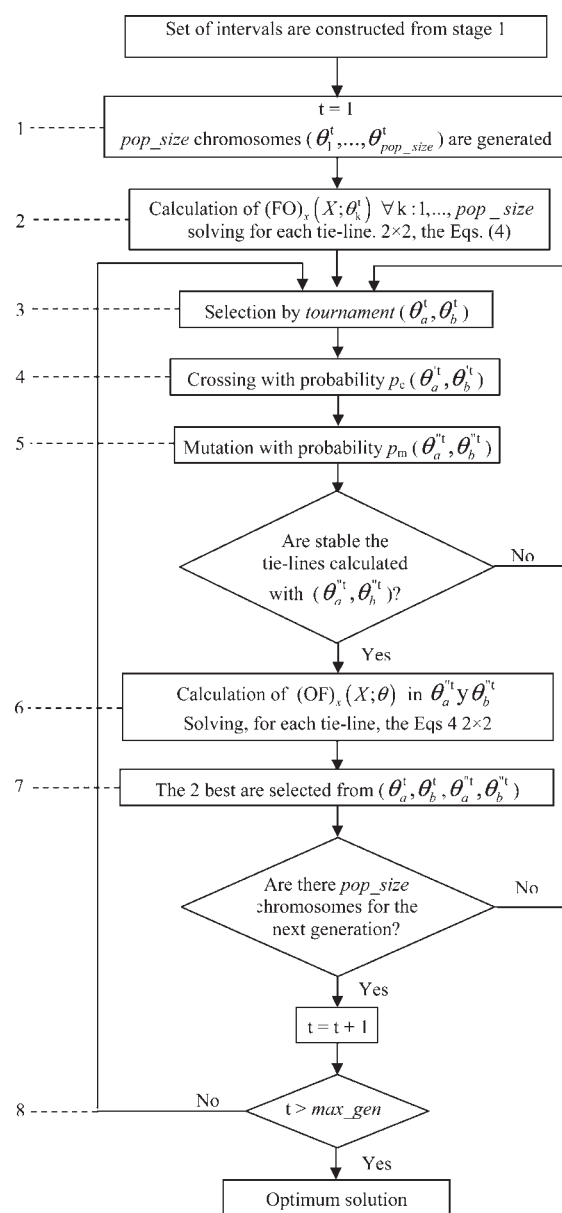


Figure A2. Flow diagram from Stage 2.

## ■ ASSOCIATED CONTENT

**S Supporting Information.** Tables S1 and S2, containing, respectively, the experimental values of solubilities and the values obtained in the application of the models eqs 10 and 16 to LLE data. This information is available free of charge via the Internet at <http://pubs.acs.org/>.

## ■ AUTHOR INFORMATION

### Corresponding Author

\*E-mail: jortega@dip.ulpgc.es.

## ■ ACKNOWLEDGMENT

This work was carried out with financial support from the Spanish MICINN (Project No. CTQ2009-12482). The authors (F.E., J.O., and L.F.) acknowledge the financial support received.

## NOMENCLATURE

### List of Symbols

$G$  = Gibbs energy function  
 $G^E$  = excess Gibbs energy function  
 $G_{ij}$  = coefficients of eqs 16 and 17  
 $GA$  = genetic algorithm  
 $g$  = adimensional Gibbs energy function  
 $g^E$  = adimensional excess Gibbs energy function  
 $g_i$  = coefficients of eqs 8 and 10  
 $g_{ij}$  = coefficients of eqs 9 and 14  
 $I, II$  = liquid phases  
 $IL$  = ionic liquid  
 $k$  = parameter of eq 11  
 $max\_gen$  = maximum number of generations for GA  
 $n_D$  = refractive index  
 $OF$  = objective function  
 $p$  = pressure  
 $p_c$  = cross probability  
 $p_m$  = mutation probability  
 $pop\_size$  = size of population in GA  
 $ppm$  = parts per million  
 $R$  = gas constant  
 $s_x$  = standard error of mole fraction (eq 15)  
 $T$  = temperature  
 $t$  = actual generation in GA  
 $UCST$  = upper critical solution temperature  
 $x$  = set of experimental data of LLE  
 $x_{IL}$  = ionic liquid mole fraction  
 $\nu$  = alkanol chain length  
 $w/w$  = weight percent  
 $Y$  = factor of eq 12, with the expression presented as eq 13  
 $z_i$  = active fraction of component  $i$  in eqs 8 and 10–13

### Cations

$[b-py]^+$  = [butylpyridinium]<sup>+</sup>  
 $[b2m-py]^+$  = [butyl-2-methylpyridinium]<sup>+</sup>  
 $[b3m-py]^+$  = [butyl-3-methylpyridinium]<sup>+</sup>  
 $[b3m-im]^+$  = [butyl-3-methylimidazolium]<sup>+</sup>  
 $[b4m-py]^+$  = [butyl-4-methylpyridinium]<sup>+</sup>  
 $[C_6OC3m-im]^+$  = [hexyloxymethyl-3-methylimidazolium]<sup>+</sup>  
 $[h-py]^+$  = [hexylpyridinium]<sup>+</sup>  
 $[h3m-im]^+$  = [hexyl-3-methylimidazolium]<sup>+</sup>  
 $[o3m-im]^+$  = [octyl-3-methylimidazolium]<sup>+</sup>

### Anions

$[BF_4]^-$  = [tetrafluoroborate]<sup>-</sup>  
 $[TF_2N]^-$  = [bis(trifluoromethylsulfonyl)imide]<sup>-</sup>

### Greek Letters

$\alpha$  = nonrandom constant of eqs 17  
 $\rho$  = density  
 $\Delta g_{ij1}, \Delta g_{ij2}, \Delta g_{ij3}$  = coefficients of eqs 16 and 17  
 $\gamma_i$  = activity coefficient of component  $i$   
 $\theta$  = set of parameters in a parametric model  
 $\tau_{ij}$  = coefficients of eqs 16 and 17

## REFERENCES

(1) Holbrey, J. D.; López-Martín, I.; Rothenberg, G.; Seddon, K. R.; Silvero, G. Desulfurisation of oils using ionic liquids: selection of cationic and anionic components to enhance extraction efficiency. *Green Chem.* **2008**, *10*, 87–92.

(2) Zhao, W.; Mo, Y.; Pu, J.; Bai, M. Effect of cation on micro/nano-tribological properties of ultra-thin ionic liquid films. *Tribol. Int.* **2009**, *42*, 828–835.

(3) Law, M. C.; Cheung, T. W.; Wong, K. Y.; Chan, T. H. Synthetic and mechanistic studies of indium-mediated allylation of imines in ionic liquids. *J. Org. Chem.* **2007**, *72*, 923–929.

(4) Ortega, J.; Vreekamp, R.; Marrero, E.; Penco, E. Thermodynamic properties of 1-butyl-3-methylpyridinium tetrafluoroborate and its mixtures with water and alkanols. *J. Chem. Eng. Data* **2007**, *52*, 2269–2276.

(5) Ortega, J.; Vreekamp, R.; Penco, E.; Marrero, E. Mixing thermodynamic properties of 1-butyl-4-methylpyridinium tetrafluoroborate [b4mpy][BF<sub>4</sub>] with water and with an alkane-1-ol (methanol to pentanol). *J. Chem. Thermodyn.* **2008**, *40*, 1087–1094.

(6) Navas, A.; Ortega, J.; Vreekamp, R.; Marrero, E.; Palomar, J. Experimental thermodynamic properties of 1-butyl-2-methylpyridinium tetrafluoroborate [b2mpy][BF<sub>4</sub>] with water and with alkan-1-ol and their interpretation with the COSMO-RS methodology. *Ind. Eng. Chem. Res.* **2009**, *48*, 2678–2690.

(7) Vreekamp, R.; Castellano, D.; Palomar, J.; Ortega, J.; Espiau, F.; Fernández, L.; Penco, E. Thermodynamic Behavior of the Binaries 1-Butylpyridinium Tetrafluoroborate with Water and Alkanols: Their Interpretation Using <sup>1</sup>H NMR Spectroscopy and Quantum-Chemistry Calculations. *J. Phys. Chem. B* **2011**, *115*, 8763–8774.

(8) Renon, H.; Praustnitz, J. M. Local compositions in thermodynamic excess functions for liquid mixtures. *AIChE J.* **1968**, *14*, 135–144.

(9) Ortega, J.; Espiau, F.; Wisniak, J. New parametric model to correlate the Gibbs excess function and other thermodynamic properties of multicomponent systems. Application to binary systems. *Ind. Eng. Chem. Res.* **2010**, *49*, 406–421.

(10) Espiau, F.; Ortega, J.; Penco, E.; Wisniak, J. Advances in the correlation of thermodynamic properties of binary systems applied to methanol mixtures with butyl esters. *Ind. Eng. Chem. Res.* **2010**, *49*, 9548–9558.

(11) Marcilla, A.; Olaya, M. M.; Serrano, M. D. Liquid–liquid equilibrium data regression. Comments. *J. Chem. Eng. Data* **2007**, *52*, 2538–2541.

(12) Riddick, J. A.; Bunger, W. B.; Sakano, T. K. *Organic Solvents: Physical Properties and Methods of Purification*, 4th ed.; Techniques of Chemistry, Vol. 2; Wiley–Interscience: New York, 1986.

(13) Wilhoit, R. C.; Zwolinski, B. J. Physical and Thermodynamic Properties of Aliphatic Alcohols. *J. Phys. Chem. Ref. Data* **1973**, *2* (Suppl. 1).

(14) Garcia-Mardones, M.; Perez-Gregorio, V.; Guerrero, H.; Bandres, I.; Lafuente, C. Thermodynamic study of binary mixtures containing 1-butylpyridinium tetrafluoroborate and methanol, or ethanol. *J. Chem. Thermodyn.* **2010**, *42*, 1500–1505.

(15) Bandrés, I.; Giner, B.; Artigas, H.; Royo, F. M.; Lafuente, C. Thermophysical Comparative Study of Two Isomeric Pyridinium-Based Ionic Liquids. *J. Phys. Chem. B* **2008**, *112*, 3077–3084.

(16) Crosthwaite, J. M.; Muldoon, M. J.; Aki, S. N. V. K.; Maginn, E. J.; Brennecke, J. F. Liquid Phase Behavior of Ionic Liquids with Alcohols: Experimental Studies and Modeling. *J. Phys. Chem. B* **2006**, *110*, 9354–9361.

(17) Crosthwaite, J. M.; Aki, S. N. V. K.; Maginn, E. J.; Brennecke, J. F. Liquid Phase Behavior of Imidazolium-Based Ionic Liquids with Alcohols. *J. Phys. Chem. B* **2004**, *108*, 5113–5119.

(18) Crosthwaite, J. M.; Aki, S. N. V. K.; Maginn, E. J.; Brennecke, J. F. Liquid phase behavior of imidazolium-based ionic liquids with alcohols: Effect of hydrogen bonding and non-polar interactions. *Fluid Phase Equilib.* **2005**, *228–229*, 303–309.

(19) Huo, Y.; Xia, S.; Ma, P. Solubility of Alcohols and Aromatic Compounds in Imidazolium-Based Ionic Liquids. *J. Chem. Eng. Data* **2008**, *53*, 2535–2539.

(20) Wagner, M.; Stanga, O.; Schroer, W. Corresponding states analysis of the critical points in binary solutions of room temperature ionic liquids. *Phys. Chem. Chem. Phys.* **2003**, *5*, 3943–3950.

(21) Heintz, A.; Klasen, D.; Lehmann, J. K.; Wertz, C. Excess molar volumes and Liquid–Liquid equilibria of the ionic liquid

1-methyl-3-octyl-imidazolium tetrafluoroborate mixed with butan-1-ol and pentan-1-ol. *J. Solution Chem.* **2005**, *34*, 1135–1144.

(22) Domanska, U.; Marciniak, A. Phase behavior of 1-hexyloxy-methyl-3-methyl-imidazolium and 1,3-dihexyloxymethyl-imidazolium based ionic liquids with alcohols, water, ketones and hydrocarbons: The effect of cation and anion on solubility. *Fluid Phase Equilib.* **2007**, *260*, 9–18.

(23) Heintz, A.; Lehmann, J. K.; Wertz, C. Thermodynamic Properties of Mixtures Containing Ionic Liquids. 3. Liquid-Liquid Equilibria of Binary Mixtures of 1-Ethyl-3-methylimidazolium Bis(trifluoromethylsulfonyl)imide with Propan-1-ol, Butan-1-ol, and Pentan-1-ol. *J. Chem. Eng. Data* **2003**, *48*, 472–474.

(24) Heintz, A.; Lehmann, J. K.; Wertz, C.; Jacquemin, J. Thermodynamic Properties of Mixtures Containing Ionic Liquids. 4. LLE of Binary Mixtures of [C<sub>2</sub>MIM][NTf<sub>2</sub>] with Propan-1-ol, Butan-1-ol, and Pentan-1-ol and [C<sub>4</sub>MIM][NTf<sub>2</sub>] with Cyclohexanol and 1,2-Hexanediol Including Studies of the Influence of Small Amounts of Water. *J. Chem. Eng. Data* **2005**, *50*, 956–960.

(25) Domanska, U.; Marciniak, A. Solubility of Ionic Liquid [emim][PF<sub>6</sub>] in Alcohols. *J. Phys. Chem. B.* **2004**, *108*, 2376–2382.

(26) Pereiro, A. B.; Rodríguez, A. Study on the phase behavior and thermodynamic properties of ionic liquids containing imidazolium cation with ethanol at several temperatures. *J. Chem. Thermodyn.* **2007**, *39*, 978–989.

(27) Sahandzhieva, K.; Tuma, D.; Breyer, S.; Pérez-Salado, A.; Maurer, G. Liquid–Liquid Equilibrium in Mixtures of the Ionic Liquid 1-*n*-Butyl-3-methylimidazolium Hexafluorophosphate and an Alkanol. *J. Chem. Eng. Data* **2006**, *51*, 1516–1525.

(28) Marsh, K. N.; Deev, A.; Wu, A. C.-T.; Tran, E.; Klamt, A. Room temperature ionic liquids as replacements for conventional solvents—A review. *Korean J. Chem. Eng.* **2002**, *19*, 357–362.

(29) Pereiro, A. B.; Rodríguez, A. Experimental Liquid-Liquid Equilibria of 1-Alkyl-3-methylimidazolium Hexafluorophosphate with 1-Alcohols. *J. Chem. Eng. Data* **2007**, *52*, 1408–1412.

(30) Lachwa, J.; Morgado, P.; Esperanca, J. M. S. S.; Guedes, H. J. R.; Lopes, J. N. C.; Rebelo, L. P. N. Fluid-Phase Behavior of {1-Hexyl-3-methylimidazolium Bis(trifluoromethylsulfonyl) Imide, [C<sub>6</sub>mim][NTf<sub>2</sub>], + C<sub>2</sub>–C<sub>8</sub> *n*-Alcohol} Mixtures: Liquid–Liquid Equilibrium and Excess Volumes. *J. Chem. Eng. Data* **2006**, *51*, 2215–2221.

(31) Domańska, U.; Marciniak, A.; Królikowski, M. Phase Equilibria and Modeling of Ammonium Ionic Liquid, C<sub>2</sub>NTf<sub>2</sub>, Solutions. *J. Phys. Chem. B* **2008**, *112*, 1218–1225.

(32) Domanska, U.; Casas, L. Solubility of phosphonium ionic liquid in alcohols, benzene, and alkylbenzenes. *J. Phys. Chem. B* **2007**, *111*, 4109–4115.

(33) Wu, C. T.; Marsh, K. N.; Deev, A. V.; Boxall, J. A. Liquid–Liquid Equilibria of Room-Temperature Ionic Liquids and Butan-1-ol. *J. Chem. Eng. Data* **2003**, *48*, 486–491.

(34) *Simulation Software: ASPEN PLUS of ASPENTECH, Aspen Physical Property System 2004.1 Physical Property Methods and Models*; Aspen Technology, Inc.: Cambridge, MA.

(35) Ko, M.; Im, J.; Sung, J. Y.; Kim, H. Liquid–Liquid Equilibria for the Binary Systems of Sulfolane with Alkanes. *J. Chem. Eng. Data* **2007**, *52*, 1464–1467.

(36) Goldberg, D. E. Genetic Algorithms in Search. In *Optimization and Machine Learning*; Addison–Wesley: New York, 1989.